

Phase Separation and Self-Assembly of Cyclic Amphiphilic Block Copolymers with a Main-Chain Liquid Crystalline Segment†

Satoshi Honda,‡ Maito Koga, Masatoshi Tokita,* Takuya Yamamoto,* and Yasuyuki Tezuka*

Department of Organic and Polymeric Materials, Tokyo Institute of Technology, O-okayama, Meguro-ku, Tokyo 152–8552, Japan

† Electronic Supplementary Information (ESI) available: SEC traces, ¹H NMR spectra, DSC thermograms, Supporting Table, WAXD intensity profiles, TEM images, a photograph for the experimental setup to apply an electric field. See DOI: ????????

‡ Present Address: Department of Industrial Chemistry, Faculty of Engineering, Tokyo University of Science, 12–1 Ichigaya–Funagawara, Shinjuku, Tokyo 162–0826, Japan.

A series of linear and cyclized amphiphilic block copolymers consisting of poly(acrylic acid) (AA_m) and main-chain liquid crystalline (LC) poly(3-methylpentamethylene-4,4'-bibenzoate) (BB_n) segments were newly synthesized. Solid state morphology was investigated by X-ray scattering. Linear AA₂₁BB₉AA₂₁, cyclic AA₃₃BB₁₀, and cyclic AA₅₁BB₁₈ formed lamellar microdomains, where the BB_n segment of cyclic AA₅₁BB₁₈ formed a smectic CA phase. On the other hand, the cylinder-type microdomains were formed by linear AA₄₄BB₉AA₄₄ and cyclic AA₁₀₀BB₉. These amphiphilic block copolymers were self-assembled in water to form vesicles or cylindrical micelles, depending on the polymer concentration of the initial THF solution. The response of these nanostructures against an electric field demonstrated that the

vesicles formed from linear AA₂₅BB₁₄AA₂₅ and cyclic AA₅₁BB₁₈ turned into substantially larger aggregates likely due the reorganization of the LC segment in the bilayer.

Introduction

Liquid crystalline (LC) polymers are arguably one of the most widely studied polymeric materials for applications such as indicating and recording elements. Owing to the rigidity and dielectric anisotropy of the polymer chain, LC polymeric materials exhibit a sensitive response to an electric or magnetic field by the macroscopic alignment of microdomains.¹ Side-chain LC segments were sometimes block copolymerized with incompatible segments to exhibit combinational functions with phase separation.² Moreover, living polymerization techniques allowed to provide amphiphilic block copolymers with a side-chain LC segment as the hydrophobe.^{3, 4} Notably, an amphiphile having a polyacrylate derivative segment appending an azobenzene functionality exhibited light-responsive order–disorder of the vesicular bilayer via the cis–trans conformational change.⁴ However, no studies have reported self-assembly of an amphiphilic block copolymer with a main-chain LC segment and electric or magnetic field-responsive properties to take full advantage of the LC segment.

In the meantime, cyclization of a series of linear compounds with biphenyl functionalities resulted in different LC transition behaviors despite no significant changes in the chemical structure or molecular weight.⁵ Furthermore, we previously reported that self-assembly of a cyclized amphiphilic block copolymer resulted in the drastic enhancement of *topology effects* on the thermal and salt stability of the micelles in comparison with those from the linear prepolymer.⁶ Therefore, the self-assembly of a cyclic amphiphilic block copolymer involving a LC segment was expected to lead to the enhancement of *topology effects* on the LC functionalities of the aggregate including a response to an electric or magnetic field.

Here linear amphiphilic triblock copolymers and their cyclized counterparts were synthesized

composed of hydrophilic poly(acrylic acid) (AA_n) segments and a hydrophobic poly(3-methylpentamethylene-4,4'-bibenzoate) (BB_n) segment, one of the most studied main-chain LC.⁷⁻⁹ Their solid state morphologies and phase transition behaviors in the LC segments of these amphiphilic block copolymers were studied. Furthermore, self-assembly in water was performed to give vesicles and cylindrical micelles depending on the conditions. Interestingly, the respective nanostructures responded to an electric field to transform to larger vesicles and an agglomerated network structure.

Experimental

Materials

All commercial reagents were used as received unless otherwise noted. THF (>99.0%, Kanto Chemical Co., Inc.) was distilled over Na wire. *tert*-Butyl acrylate (*t*BA) was passed through an alumina column to remove the inhibitor and bubbled with dry nitrogen for 30 min. Hydroxy-terminated BB_n (molecular weight by ^1H NMR, $M_n = 1700$) was synthesized according to the literature.⁹ A bromo-terminated bifunctional polystyrene macroinitiator was synthesized by atom transfer radical polymerization (ATRP) of styrene from benzal bromide.¹⁰ Poly(acrylic acid)-polystyrene-Poly(acrylic acid) ($AA_{134}St_{34}AA_{134}$) was prepared by ATRP of *t*BA from a polystyrene macroinitiator and subsequent hydrolysis of the *tert*-butyl groups according to the reported procedure.¹¹

Synthesis of BB_n Macroinitiators

BB_n macroinitiators having bromoisobutyryl groups at the chain ends were synthesized through esterification of hydroxy-terminated BB_n with 2-bromoisobutyryl bromide according to a modified procedure in the literature.⁹ Thus, into an anhydrous CH_2Cl_2 solution (100 mL) of hydroxy-terminated BB_n (10.0 g, 5.7 mmol, $M_n = 1700$) and triethylamine (10.4 mL, 75 mmol),

2-bromoisobutyryl bromide (7.65 mL, 62 mmol) was added dropwise at 0 °C. The solution was allowed to warm to room temperature and stirred for 19 h under nitrogen atmosphere. The reaction mixture was filtered and poured into water (100 mL), and the aqueous phase was extracted by three portions of CH₂Cl₂ (100 mL). The combined organic extract was evaporated to dryness under reduced pressure, and the residue was reprecipitated into MeOH to give a BB_n macroinitiator (7.0 g, 2.5 mmol, $M_n = 2800$) in 43% yield. ¹H NMR (300 MHz, CDCl₃) δ : 1.02–1.15 (m, –CH₂CH(CH₃)CH₂–), 1.60–2.00 (m, –CH₂CH(CH₃)CH₂–, –OC(=O)C(CH₃)₂Br), 4.26 (m, –CH₂CH₂OC(=O)C(CH₃)₂Br), 4.36–4.51 (m, –CH₂CH₂OC(=O)Ar–), 7.51–7.65 (m, ArH meta to –CO₂–), 8.00–8.12 (m, ArH ortho to –CO₂–).

The obtained BB_n macroinitiator was fractionated by preparative size exclusion chromatography (SEC) with THF as an eluent at a flow rate of 14 mL/min. The SEC trace of the fractionated BB₉ macroinitiator ($M_n = 3400$) showed a narrow polydispersity index (PDI = 1.16) but a multimodal peak (peak molecular weight by SEC calibrated with polystyrene standards, $M_p = 3800, 3200, 2700, \text{ and } 2200$, Figure S1a). The intervals of the multimodal peak corresponded to the BB_n monomer unit ($M = 324.37$). The BB₉ macroinitiator was used for the synthesis of linear *t*BA₂₁BB₉*t*BA₂₁ and linear *t*BA₅₀BB₈*t*BA₅₀. A BB₁₄ macroinitiator ($M_n = 4900, M_p = 7300, \text{ PDI} = 1.13$) was also obtained by SEC fractionation and used for the synthesis of linear *t*BA₂₇BB₁₈*t*BA₂₇.

Block Copolymerization and Allylation

The SEC-fractionated BB₉ macroinitiator (458 mg, 0.13 mmol, $M_n = 3400$, CuBr (36 mg, 0.25 mmol), *t*BA (5.0 mL, 34 mmol), toluene (5.0 mL) were added to a test tube, and the mixture was degassed by three freeze–pump–thaw cycles. The suspension was stirred at 120 °C, and *N,N,N',N'',N'''*-pentamethyldiethylenetriamine, PMDETA, (53 μ L, 0.25 mmol) was added. The resulting suspension was stirred at 120 °C for 15 min. The reaction mixture was quenched in liquid nitrogen and allowed to warm to room temperature. The remaining monomer was removed under reduced pressure,

and allyltributylstannane (0.84 mL, 2.7 mmol) and toluene (5 mL) were added to the residue. The resulting suspension was degassed by three freeze–pump–thaw cycles and stirred at 110 °C for 17 h under vacuum. The reaction mixture was precipitated into cold *n*-hexane, and the solid obtained was filtered through a plug of alumina using CHCl₃ as an eluent. The crude product was fractionated by preparative SEC with CHCl₃ as an eluent at a flow rate of 3.5 mL/min and reprecipitated in *n*-hexane to allow isolation of linear *t*BA₂₁BB₉*t*BA₂₁ (558 mg) in 49% yield. M_n (NMR) = 2600–2800–2600, M_p = 10800, PDI = 1.16. ¹H NMR (300 MHz, CDCl₃) δ : 0.98–1.14 (m, –CH₂CH(CH₃)CH₂–), 1.17–2.00 (m, –CH₂CH(CH₃)CH₂–, –OC(=O)C(CH₃)₂–, –CH₂CH(CO₂*t*Bu)–, –CO₂C(CH₃)₃, –CH₂CH=CH₂), 2.11–2.32 (m, –CH₂CH(CO₂*t*Bu)–), 4.10 (m, 4H, –CH₂CH₂OC(=O)C(CH₃)₂–), 4.32–4.50 (m, –CH₂CH₂OC(=O)Ar–), 4.94–5.07 (m, 4H, –CH₂CH=CH₂), 5.68 (m, 2H, –CH₂CH=CH₂), 7.49–7.64 (m, ArH meta to –CO₂–), 7.98–8.11 (m, ArH ortho to –CO₂–).

Likewise, linear *t*BA₂₇BB₁₈*t*BA₂₇ and linear *t*BA₅₀BB₈*t*BA₅₀ were synthesized from the BB₁₄ and BB₉ macroinitiators, respectively. After block copolymerization and allylation, each reaction mixture was precipitated into cold MeOH. The solid obtained was filtered through a plug of alumina using CHCl₃ as an eluent to allow isolation of linear *t*BA₂₇BB₁₈*t*BA₂₇ and linear *t*BA₅₀BB₈*t*BA₅₀.

Metathesis Polymer Cyclization (MPC)

The second-generation Hoveyda–Grubbs catalyst (92 mg, 0.15 mmol) was added to a toluene solution (800 mL) of linear *t*BA₂₁BB₉*t*BA₂₁ (200 mg, 24 μ mol), and the resulting solution was stirred at 80 °C for 40 h. Ethyl vinyl ether (10 mL) was added to the reaction mixture to quench the catalyst, and the color of the solution immediately changed from brown–green to dark brown. The resulting suspension was stirred for 10 min at 80 °C. After cooling to room temperature, the reaction mixture was concentrated under reduced pressure and filtered through a plug of alumina using CHCl₃ as an eluent. The crude product was fractionated by preparative SEC with CHCl₃ as an eluent at a flow rate of 3.5

mL/min to allow isolation of cyclic $tBA_{31}BB_{10}$ (140 mg) in 78% yield. M_n (NMR) = 4000–3300, M_p = 9200, PDI = 1.24. 1H NMR (300 MHz, $CDCl_3$) δ : 0.97–1.15 (m, $-CH_2CH(CH_3)CH_2-$), 1.18–2.00 (m, $-CH_2CH(CH_3)CH_2-$, $-OC(=O)C(CH_3)_2-$, $-CH_2CH(CO_2tBu)-$, $-CO_2C(CH_3)_3$, $-CH_2CH=CHCH_2-$), 2.10–2.32 (m, $-CH_2CH(CO_2tBu)-$), 4.10 (m, 4H, $-CH_2CH_2OC(=O)C(CH_3)_2-$), 4.34–4.50 (m, $-CH_2CH_2OC(=O)Ar-$), 5.30 (m, 2H, $-CH_2CH=CHCH_2-$), 7.46–7.64 (m, ArH meta to $-CO_2-$), 7.96–8.11 (m, ArH ortho to $-CO_2-$).

Likewise, cyclic $tBA_{54}BB_{16}$ and cyclic $tBA_{91}BB_8$ were synthesized.

Hydrolysis of Linear tBA_mBB_n and Cyclic $tBA_{2m}BB_n$

Linear $tBA_{21}BB_9$ (50 mg, 5.9 μ mol) was dissolved in CH_2Cl_2 (10 mL), and trifluoroacetic acid (TFA, 1.9 mL, 25 mmol) was added. The mixture was stirred at room temperature for 14 h under nitrogen atmosphere. The reaction mixture was concentrated under reduced pressure and precipitated into $CHCl_3$ to allow isolation of linear $AA_{21}BB_9AA_{21}$ (35 mg) in 92% yield. M_n (NMR) = 1500–3000–1500, 1H NMR (300 MHz, CF_3COOD) δ : 0.98–1.41 (m, $-CH_2CH(CH_3)CH_2-$), 1.47–2.39 (m, $-CH_2CH(CH_3)CH_2-$, $-OC(=O)C(CH_3)_2-$, $-CH_2CH(CO_2H)-$, $-CH_2CH=CH_2$), 2.50–2.99 (m, $-CH_2CH(CO_2H)-$), 4.22 (m, $-CH_2CH_2OC(=O)C(CH_3)_2-$), 4.33–4.70 (m, $-CH_2CH_2OC(=O)Ar-$), 4.98–5.13 (m, 4H, $-CH_2CH=CH_2$), 5.67 (m, 2H, $-CH_2CH=CH_2$), 7.36–7.67 (m, ArH meta to $-CO_2-$), 7.86–8.34 (m, ArH ortho to $-CO_2-$).

The hydrolysis of cyclic $tBA_{31}BB_{10}$ was carried out in the same procedure to give cyclic $AA_{33}BB_{10}$ in 85% yield. M_n (NMR) = 2400–3400, 1H NMR (300 MHz, CF_3COOD) δ : 0.94–1.43 (m, $-CH_2CH(CH_3)CH_2-$), 1.48–2.30 (m, $-CH_2CH(CH_3)CH_2-$, $-OC(=O)C(CH_3)_2-$, $-CH_2CH(CO_2H)-$, $-CH_2CH=CHCH_2-$), 2.59–2.85 (m, $-CH_2CH(CO_2H)-$), 4.22 (m, $-CH_2CH_2OC(=O)C(CH_3)_2-$), 4.39–4.65 (m, $-CH_2CH_2OC(=O)Ar-$), 5.48 (m, 2H, $-CH_2CH=CHCH_2-$), 7.30–7.63 (m, ArH meta to $-CO_2-$), 7.80–8.09 (m, ArH ortho to $-CO_2-$).

Likewise, linear AA₂₅BB₁₄AA₂₅, cyclic AA₅₁BB₁₈, linear AA₄₄BB₉AA₄₄, and cyclic AA₁₀₀BB₉ were synthesized.

NMR Measurements

¹H NMR spectra were recorded at room temperature on a JEOL JNM-AL300 spectrometer operating at 300 MHz. CDCl₃ or CF₃COOD was used as a solvent, and chemical shifts were reported relative to the signal of the residual proton of the deuterated solvent.

SEC Measurements

SEC measurements were performed at 40 °C on a HPLC system equipped with a Tosoh CCPS pump, Tosoh TSK G3000HXL column, and Tosoh RI 8020 refractive index detector. THF was used as an eluent at a flow rate of 1.0 mL/min. Linear polystyrene standards were used for calibration, and the *M*_p values were reported as polystyrene equivalents.

SEC Fractionation

SEC fractionation was performed on a JAI LC-908 recycling preparative HPLC system equipped with JAIGEL-2H and JAIGEL-3H columns using CHCl₃ as an eluent at a flow rate of 3.5 mL/min or a JAI LC-9204 recycling preparative HPLC system equipped with two of JAIGEL-2H-40, JAIGEL-3H-40, and JAIGEL-4H-40 columns using THF as an eluent at a flow rate of 14 mL/min.

X-Ray Measurements

Wide-angle X-ray diffraction (WAXD) patterns were measured by a Bruker D8 DISCOVER equipped with a Vantec-500 detector using Cu K radiation. The synchrotron radiation (SR)-SAXS measurement was performed at a BL-10C beamline in Photon Factory, Tsukuba, Japan, equipped with

PILATUS3 2M. The X-ray wavelength (λ) was 0.1488 nm, and the camera length was 2 m. The scattering intensity was plotted against the scattering vector $q = 4\pi \sin \theta/\lambda$. For the preparation of a specimen, an amphiphilic block copolymer was dissolved in THF, and the solvent was slowly dried.

DSC Measurements

Differential scanning calorimetry (DSC) was performed using a PerkinElmer Pyris 1 DSC calorimeter equipped with an Intracooler II under a flow of dry nitrogen. The same specimen preparation method for the X-ray measurements was used.

Self-Assembly

Distilled water (1.0 mL) was slowly added to a vigorously stirred THF solution of linear $AA_mBB_nAA_m$ or cyclic $AA_{2m}BB_n$ (either $c_0 = 1.0$ mg/mL, 1.0 mL or $c_0 = 10$ mg/mL, 0.10 mL, where c_0 indicates the polymer concentration of the initial THF solution). THF was removed under reduced pressure, and the resulting suspension was diluted with distilled water to a total volume of 1.0 mL to form a 1.0 mg/mL aqueous suspension of linear $AA_mBB_nAA_m$ or cyclic $AA_{2m}BB_n$. On the other hand, distilled water (1.0 mL) was added to $AA_{134}St_{34}AA_{134}$ (10 mg), and the mixture was sonicated. The resulting suspension was diluted with distilled water to a total volume of 10 mL to form a 1.0 mg/mL aqueous suspension of $AA_{134}St_{34}AA_{134}$.

TEM Observations

A carbon-coated Formvar film supported by a Cu grid (200 mesh) was plasma glow discharged for 60 s to form a hydrophilic surface. An aqueous suspension (10 μ L) of linear $AA_mBB_nAA_m$, cyclic $AA_{2m}BB_n$, or linear $AA_{134}St_{34}AA_{134}$ was placed on the film, and the excess suspension was removed with a filter paper. For the TEM images of Figures 3e and 3f, the samples on the films were stained.

Thus, a TI-blue solution (Nisshin EM) was diluted to 5-fold with water. The diluted solution (10 μ L) was placed on a sample-loaded film for 60 s and removed with a filter paper. The sample-loaded films with and without staining were carefully dried under reduced pressure. TEM observations were performed on a Hitachi H-7650 Zero A microscope operating at 60 kV.

Results and discussion

Synthesis

Macroinitiators possessing a BB_n functionality were prepared by esterification of hydroxy-terminated BB_n ($M_n = 1700$) with 2-bromoisobutyryl bromide as reported (Scheme 1a).⁹ The quantitative conversion of the hydroxyl groups into bromoisobutyryl groups was confirmed by the replacement of the ^1H NMR signal of the hydroxyl-adjacent methylene groups at 3.73 ppm (“g” in Figure S2a) by the ester neighboring the methylene proton at 4.26 ppm (“g” in Figure S2b). The product was fractionated by SEC to give BB_9 ($M_n = 3400$, $M_p = 3800, 3200, 2700$, and 2200 , PDI = 1.16 in Figure S1a) and BB_{14} ($M_n = 4900$, $M_p = 7300$, PDI = 1.13) macroinitiators. The intervals of the multimodal peak of the BB_9 macroinitiator corresponded to the BB_n monomer unit ($M = 324.37$).

Allyl-telechelic block copolymers were prepared through ATRP of *t*BA from the BB_n macroinitiators in the presence of CuBr and PMDETA followed by allylation of the terminal bromides with allyltributylstannane (Scheme 1a). The effective end-capping reaction was confirmed by the ^1H NMR signals “m” at 5.68 ppm and “n” at 4.94–5.07 ppm for allyl-terminated linear $tBA_{21}BB_9tBA_{21}$ (Figure S3a). In addition, the signals from the two phenylene groups in the BB_n units at 7.98–8.11 ppm for “e” and 7.49–7.64 ppm for “f” and the large signal due to the *tert*-butyl protons at 1.42 ppm for “k” were observed. SEC traces of a BB_9 macroinitiator ($M_p = 3800, 3200, 2700$, and 2200 , PDI = 1.16 in Figure S1a) and linear $tBA_{21}BB_9tBA_{21}$ ($M_p = 10800$, PDI = 1.16 in Figure S1b) were compared to show the shift toward the higher molecular weight region with retaining narrow polydispersity, which was

indicative of living polymerization. Moreover, the molecular weight of tBA_m segments increased along with the polymerization time (Table 1).

Allyl-telechelic $tBA_mBB_n tBA_m$ was subjected to the metathesis polymer cyclization (MPC) process under the dilution (0.25 g/L) in the presence of the second-generation Hoveyda–Grubbs catalyst.^{6,12} The 1H NMR spectra of the product from linear $tBA_{21}BB_9 tBA_{21}$ showed the signals of the inner olefinic group at 5.30 ppm for both cis and trans isomers (“m” in Figure S3c), completely replacing those from the terminal allyl groups of the prepolymer (“m” and “n” in Figure S3a). In addition, the other signals were essentially unaffected through MPC, indicating no side reactions occurred in the present reaction system. The molecular weights of the prepolymer and product determined by 1H NMR (M_n), and thus their formulae (linear $tBA_mBB_n tBA_m$ and cyclic $tBA_{2m}BB_n$), were somewhat inconsistent with each other due to the purification process to remove intermolecularly coupled products (Table 1).

SEC for cyclic $tBA_{31}BB_{10}$ showed a unimodal peak in the absence of a noticeable shoulder at the higher molecular weight region after fractionation by preparative SEC ($M_p = 9200$ in Figure S1c). The results of MPC with linear $tBA_{27}BB_{18} tBA_{27}$ and linear $tBA_{50}BB_8 tBA_{50}$ are also summarized in Table 1. While the linear precursors with a relatively short BB_n segment (linear $tBA_{21}BB_9 tBA_{21}$ and linear $tBA_{50}BB_8 tBA_{50}$) showed high yields ($\geq 70\%$), that of linear $tBA_{27}BB_{18} tBA_{27}$ was comparably low (38%). This was expected to be caused by the suppressed intramolecular metathesis of the latter having the longer rigid BB_n segment. Nevertheless, the present cyclization process is applicable for a linear $tBA_mBB_n tBA_m$ precursor with rather high molecular weight (~ 15000 for linear $tBA_{50}BB_8 tBA_{50}$) with the appropriate length of the BB_n segment.

The tBA_m segments were hydrolyzed by trifluoroacetic acid (TFA) to give poly(acrylic acid), AA_m , segments in the acid form, forming linear $AA_mBB_n AA_m$ and cyclic $AA_{2m}BB_n$ amphiphilic block copolymers (Scheme 1). As reported elsewhere, a *tert*-butyl ester group is easily deprotectable by the

addition of TFA without causing a side reaction.¹³ The ¹H NMR spectra of the products, linear AA₂₁BB₉AA₂₁ (Figure S3b) and cyclic AA₃₃BB₁₀ (Figure S3d), showed the disappearance of the signal of the *tert*-butyl protons at 1.42 ppm (“k” in Figures S3a and S3c). Moreover, the signals of the allyl groups of linear *t*BA₂₁BB₉*t*BA₂₁ (“m” at 5.68 ppm and “n” at 4.94–5.07 ppm in Figure S3a) and the inner olefinic group of cyclic *t*BA₃₁BB₁₀ (“m” at 5.30 ppm in Figure S3c) as well as the other protons were unaffected through hydrolysis. Likewise, a series of linear AA_mBB_nAA_m and cyclic AA_{2m}BB_n with different molecular weights were synthesized and characterized (Table 1). Also in this synthetic process, M_n and the formulae of the copolymers shifted due to purification.

Solid State Morphology

The phase separation of these linear and cyclic amphiphilic block copolymers in the solid state was studied. Linear AA₂₁BB₉AA₂₁, cyclic AA₃₃BB₁₀, and cyclic AA₅₁BB₁₈ segregated each segment to form lamellar microdomains which display SAXS profiles including maxima at scattering vectors q at integer ratios (Figure 1). Effects of macrocyclization on the lamellar morphology can be recognized by comparing the SAXS profile of cyclic AA₃₃BB₁₀ with the linear AA₂₁BB₉AA₂₁ counterpart. The scattering peaks of the linear copolymer are broader than that for the cyclic counterpart, suggesting that the lamellae periodicity was less ordered for the linear copolymer. While the lamellar spacings (d_{100}) were comparable to each other (linear AA₂₁BB₉AA₂₁, 9.3 nm; cyclic AA₃₃BB₁₀, 9.2 nm), the LC lamella thickness estimated from the SAXS peak intensity ratios was larger for the cyclic copolymer (linear AA₂₁BB₉AA₂₁, 3.3 nm; cyclic AA₃₃BB₁₀, 5.9 nm) as shown in Table 2. Though the macrocyclization decreased M_n of the AA_m segment to increase the BB_n volume fraction by a factor of $\phi_{v, BBn, cyclic} / \phi_{v, BBn, linear} = 0.57 / 0.48 = 1.2$, the BB_n lamellar thickness increases by a factor of $5.9 \text{ nm} / 3.3 \text{ nm} = 1.8$, which was remarkably larger than that expected from the difference in $\phi_{v, BBn}$. Thus the macrocyclization by connecting the AA_m segments at both chain end decreases the AA_m lamella thickness and increases the

middle BB_n segment lamella thickness to maintain the lamellar spacing constant.

Here we note that the BB_n segments in both copolymers might form an ordered phase. Both copolymers exhibited DSC thermograms including two steps at around 55 °C and 100 °C attributed to the glass transition of BB_n and AA_m segments, respectively, and an endothermic peak at around 140 °C in the heating process (Figures S4a and S4b). The ordered phase seems to be different from the smectic CA phase formed by BB-5(3-Me) homopolymer because it exhibited higher T_g and lower T_i and smaller ΔH_i than that of the smectic CA (SmCA) phase ($T_g = 30$ °C, $T_i = 150$ °C, and $\Delta H_i = 3.8$ kJ mol⁻¹).⁸ Moreover both copolymers did not display the layer reflection characteristic to the SmCA phase with a d-spacing of 1.63 nm in the WAXD intensity profiles (Figure S5). In contrast, the BB_n segment of cyclic $AA_{51}BB_{18}$ formed the SmCA phase displaying the layer reflection with $d = 1.63$ nm in the WAXD pattern though $T_i = 111$ °C and $\Delta H_i = 2.33$ kJ mol⁻¹ (Figure S4c, Table S1) were smaller than that of the homopolymer and was accommodated in 7.1 nm thick lamellae (Table 2). The average contour length of the BB_{18} was 29.3 nm determined by a layer spacing of 1.63 nm multiplied by the number of the BB_n units. Assuming that the BB_n segments are most extended perpendicular to the lamellar interface, the BB_n segment folds at every 4.4 units in average to be accommodated in the 7.1 nm thick lamellae. The average number of folding was 3.1 ($(29.3 \text{ nm} / 7.1 \text{ nm}) - 1$). The odd number of folding may be in accord with the cyclic topology of the copolymer (Figure 2c). The lamellar microdomain structures thus elucidated are depicted in Figures 2a–c.

The pair of linear $AA_{44}BB_9AA_{44}$ and cyclic $AA_{100}BB_9$ formed cylinder-type microdomains displaying scattering peaks at q with ratios of $1:4^{0.5}:9^{0.5}$ (Figures 1d and 1e). It should be noted that $3^{0.5}$ peak is missing. This suggests that its position may correspond to the position of the first zero of the form factor. In the SAXS profiles, the square of the calculated form factor for a cylinder with 3.9 nm in radius is presented with solid line. The first zero arise at around $q = 1.0$ nm⁻¹, which corresponds to the position of the $3^{0.5}$ peak as found in Figures 1d and 1e. The distance between two adjacent cylinder

centers was estimated to be 12.7 and 12.4 nm for the linear and cyclic copolymers, respectively (Figures 2d and 2e). From the volume fractions of each segment, the BB_n segments were assumed to be accommodated within the cylinders. Both copolymers did not exhibit the endothermic peak (Figures S4d and S4e), and the layer reflection ascribed to be the smectic phase formed by the BB-5(3-Me) homopolyester (Figures 1d and 1e), suggesting that the BB_n segment is amorphous. Here the macrocyclization by connecting the AA_m segments at both chain end can decrease the volume fraction of the AA_m segments immersing the BB_n -segment cylinders. Though the BB_n volume fraction calculated from M_n of each segment was 0.30 and 0.27 for the linear and cyclic copolymers, respectively, that calculated from the dimensions of the cylinder microdomain was 0.35 for both copolymers (see Table 2).

Self-Assembly in Water

Some of the linear and cyclic amphiphilic block copolymers were self-assembled in water to determine the *topology effects* on discrete structures. Self-assembly of linear $AA_{21}BB_9AA_{21}$, linear $AA_{25}BB_{14}AA_{25}$, cyclic $AA_{33}BB_{10}$, and cyclic $AA_{51}BB_{18}$ was carried out by evaporating a good solvent from a mixture of the good solvent and water that contained an amphiphilic block copolymer,¹⁴ and the resulting nanostructure was observed by transmission electron microscopy (TEM). Thus, distilled water (1.0 mL) was slowly added to a vigorously stirred THF solution of a copolymer (1.0 mg/mL, 1.0 mL). THF was removed under reduced pressure, and distilled water was added to a total volume of 1.0 mL to form an aqueous suspension of the copolymer (1.0 mg/mL). The TEM images of suspensions containing each of self-assembled linear $AA_{21}BB_9AA_{21}$ and cyclic $AA_{33}BB_{10}$ showed a cylindrical micellar morphology with approximately 20–30 nm in width (Figures S6a and S6b). No significant difference between linear $AA_{21}BB_9AA_{21}$ and cyclic $AA_{33}BB_{10}$ was observed despite the changes in the topology and the molecular weight of the AA_m segments. On the other hand, the structure formed by linear $AA_{25}BB_{14}AA_{25}$ (Figure 3a) was quite uniform, while that observed for cyclized $AA_{51}BB_{18}$ was much

less continuous (Figure 3b). According to the critical packing parameter (CPP) theory,¹⁵ the hydrophobic/hydrophilic balance of an amphiphilic block copolymer determines the morphology of the self-assembly.^{15, 16} The concurrent formation of discrete micelles indicates that cyclic AA₅₁BB₁₈ had a significantly smaller CPP than linear AA₂₅BB₁₄AA₂₅. Despite the molecular weight fraction of the BB_n segment is larger for cyclic AA₅₁BB₁₈ ($5900/(3700 + 5900) = 0.61$) than linear AA₂₅BB₁₄AA₂₅ ($4700/(1800 + 4700 + 1800) = 0.57$) as shown in Table 1, the cyclic topology was expected to more restrict the conformational degree of freedom of the BB_n segment compared to that of the linear counterpart, resulting in a smaller CPP. Models for the cylindrical micelles are depicted in Figure S7.

The dependence of the self-assembled structure on the polymer concentration of the initial THF solution (c_0) was subsequently investigated. Generally, self-assembly is strongly influenced by the diffusion process of a poor solvent into a good solvent that solvates the less soluble segment.¹⁷ Therefore, to investigate the possible formation of other structures by controlling the diffusion kinetics, c_0 was increased to 10 mg/mL. For self-assembly of linear AA₂₁BB₉AA₂₁ (Figure S6c) and corresponding cyclic AA₃₃BB₁₀ (Figure S6d), the predominant morphology was still cylindrical micelles. Although discrete spherical micelles were observed only for linear AA₂₁BB₉AA₂₁, the effect of c_0 seemed rather small for these copolymers. In sharp contrast, the morphology of the aggregates from linear AA₂₅BB₁₄AA₂₅ and corresponding cyclic AA₅₁BB₁₈ was notably changed to vesicles. The size of the vesicles formed from cyclic AA₅₁BB₁₈ was ca. 20–200 nm in diameter with a certain degree of size distribution (Figure 3f). On the other hand, the vesicles from linear AA₂₅BB₁₄AA₂₅ were larger (mostly ca. 200 nm–500 nm in diameter, Figure 3e), and ones as large as 2 μ m were also found. TI-blue, a staining agent, was used on these vesicles to show sufficient contrast in the TEM images. Although dynamic light scattering measurements were attempted, the size distributions could not be obtained likely due to that the exceedingly large distributions did not allow for the fitting of the data. Compared to linear AA₂₁BB₉AA₂₁ and cyclic AA₃₃BB₁₀, linear AA₂₅BB₁₄AA₂₅ and cyclic AA₅₁BB₁₈ had a relatively

longer BB_n segment, which tended to form a bilayer for vesicles. The formation of vesicles from an amphiphile with a longer hydrophobic chain is consistent with the CPP theory¹⁵ as well as previous reports.^{17, 18}

Response to an electric field

Although several studies have so far been performed on the self-assembly of an amphiphilic block copolymer having a LC segment to construct discrete structures,^{3, 4} their electric or magnetic field response, which is the most characteristic properties of a LC polymer, has not been reported. To the vesicles and cylindrical micelles obtained from the present linear and cyclic LC copolymers, an electric field was applied to investigate their response. The experimental setup is shown in Figure S8. In order to prevent electrolysis of water, the effective minimal strength of the electric field (1.5 V/mm) and time (2 min) were optimized. The effects on the self-assembled structures were observed by TEM. Interestingly, the vesicles from cyclic $AA_{51}BB_{18}$ became significantly larger by applying an electric field (as large as ca. 3 μm in diameter, Figure 3h). Small vesicles of tens to hundreds nanometers were also observed at the surface of the micrometer-scale vesicles. Moreover, the bilayer was rather clearly observed even without staining. It was expected that the self-assembled vesicles transformed into the larger vesicles by the fusion of the bilayer through the reorganization of the LC segments in response to the electric field. The reorganization likely gave a thermodynamically more stable, more regulated, and robust bilayer, resulting in the significantly larger aggregate size and the clear appearance in the TEM image. For linear $AA_{25}BB_{14}AA_{25}$, vesicles with 1–2 μm in diameter were observed after applying an electric field (Figure 3g). No smaller vesicles (200 nm–500 nm) that existed in Figure 3e were found, suggesting that the small vesicles were re-assembled into the micrometer-scale vesicles. The vesicles from linear $AA_{25}BB_{14}AA_{25}$ and cyclic $AA_{51}BB_{18}$ were rather similar in size after applying an electric field than those as self-assembled. These results suggest that the topology, possibly as well as the difference in the

molecular weight of the BB_n segment caused by purification, plays a more significant role during the self-assembly process than the reorganization by an electric field. In the meantime, the cylindrical micelles formed from the respective linear and cyclic copolymers using c_0 of 1.0 mg/mL became an agglomerated network structure under the same electric field conditions (Figures 3c and 3d). The BB_n unit has dielectric anisotropy between the long and short axes of the biphenyl group, and the long axis is aligned parallel to an applied electric field. The isotropic transformation to form the larger vesicles and agglomerated network was probably caused by the rotation of the structures in the solvent. In accord with the reported transformation of vesicles by the osmotic pressure,^{17, 19} the details of the present phenomenon are currently under investigation.

Since poly(acrylic acid) is an anionic polymer, the observed electric field response could be caused by the negative surface charge of the nanostructures. To confirm the effect of the BB_n segment on the electric field response, a polystyrene (St_n) counterpart, linear $AA_{134}St_{34}AA_{134}$, was used for the electric field-applying experiment. Self-assembly gave a spherical nanostructure with 300 nm or less in diameter with a large size distribution (Figure S9a). However, this nanostructure did not show any response to an electric field (Figure S9b). Therefore, the electric field response of the vesicles and cylindrical micelles indeed arose from the BB_n segment.

Conclusions

Series of linear and cyclized amphiphilic block copolymers consisting of hydrophilic AA_m and hydrophobic BB_n segments were synthesized, where BB_n is a typical main-chain LC. The phase separation in the solid state was studied on the basis of the topology and segment lengths of the copolymers. The self-assembly in water led to the formation of vesicles or cylindrical micelles depending on c_0 . The application of an electric field resulted in the reorganization of the BB_n segment, giving rise to the transformation to micrometer-scale vesicles or an agglomerated network structure. The

utilization of the present methodology would widely open the applications of voltage-sensing materials. Furthermore, the amphiphilic block copolymers having a main-chain LC segment reported here resemble voltage sensor-containing phosphatase (VSP) for ion channels and transporters.^{20, 21} Therefore, the dynamic motions upon applying an electric field would mimic the VSP functions of the cell membrane to deliver electric signals.²⁰

Acknowledgements

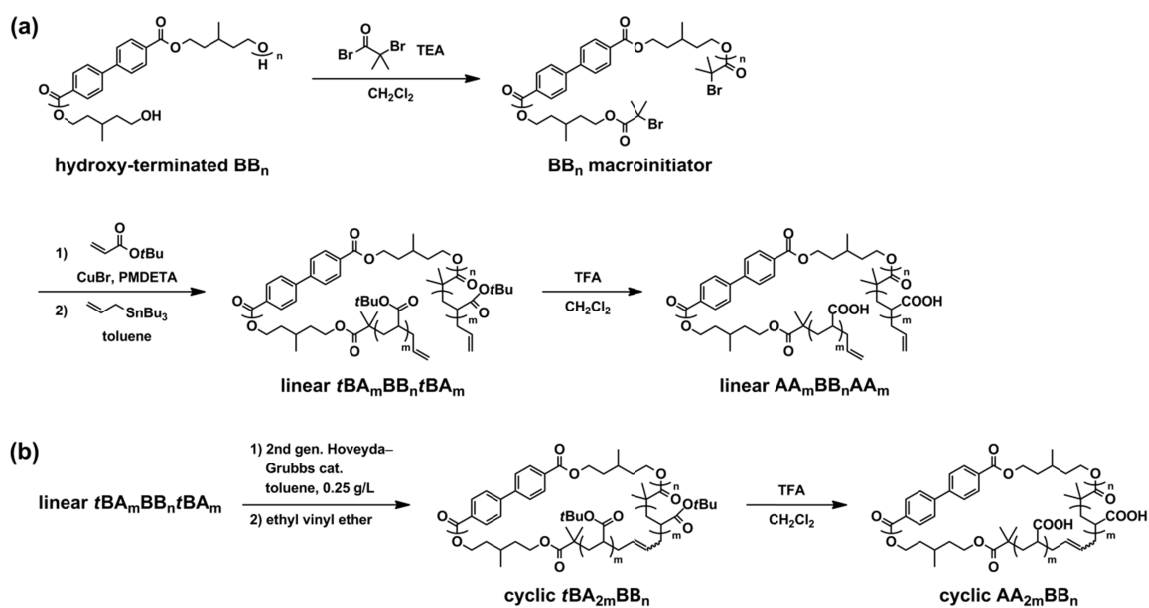
The authors are grateful to Prof. M. Kakimoto for access to NMR facilities. We thank the Center for Advanced Materials Analysis, Technical Department, Tokyo Institute of Technology for TEM observations. This work was supported by the Grant-in-Aid for JSPS Fellows (24·9031, S.H.), Mizuho Foundation for the Promotion of Sciences (S.H.), Global COE Program (Education and Research Center for Material Innovation), MEXT, Japan (S.H.), and KAKENHI (26288099 T.Y.). The SR-SAXS measurement has been performed under the approval of the Photon Factory Program Advisory Committee (No. 2013G544).

References

- 1 A. M. Donald, A. H. Windle, S. Hanna, *Liquid Crystalline Polymers*, 2nd ed., Cambridge University Press, Cambridge, U.K., 2006.
- 2 (a) W. Y. Zheng, P. T. Hammond, *Macromol. Rapid Commun.*, 1996, **17**, 813-824; (b) M. Petr, B.-a. Katzman, W. DiNatale, P. T. Hammond, *Macromolecules*, 2013, **46**, 2823-2832.
- 3 (a) C. Osuji, P. J. Ferreira, G. Mao, C. K. Ober, J. B. Vander Sande, E. L. Thomas, *Macromolecules*, 2004, **37**, 9903-9908; (b) J. Yang, D. Levy, W. Deng, P. Keller, M. H. Li, *Chem. Commun.*, 2005, 4345-4347; (c) H. Yu, A. Shishido, T. Ikeda, T. Iyoda, *Macromol. Rapid Commun.*, 2005, **26**, 1594-1598; (d) E. Mabrouk, D. Cuvelier, L.-L. Pontani, B. Xu, D. Levy, P. Keller, F. Brochard-Wyart,

- P. Nassoy, M.-H. Li, *Soft Matter*, 2009, **5**, 1870-1878.
- 4 B. Yan, X. Tong, P. Ayotte, Y. Zhao, *Soft Matter*, 2011, **7**, 10001-10009.
- 5 M. Itoh, M. Tokita, K. Adachi, T. Hayakawa, S. Kang, Y. Tezuka, J. Watanabe, *Liq. Cryst.*, 2009, **36**, 1443-1450.
- 6 (a) S. Honda, T. Yamamoto, Y. Tezuka, *J. Am. Chem. Soc.*, 2010, **132**, 10251-10253; (b) S. Honda, T. Yamamoto, Y. Tezuka, *Nat. Commun.*, 2013, **4**, 1574.
- 7 (a) J. Watanabe, M. Hayashi, A. Morita, M. Tokita, *Macromolecules*, 1995, **28**, 8073-8079; (b) J. Watanabe, M. Hayashi, M. Tokita, *React. Funct. Polym.*, 1996, **30**, 191-196; (c) M. Tokita, K. Osada, J. Watanabe, *Polym. J.*, 1998, **30**, 589-595.
- 8 (a) K. Osada, H. Niwano, M. Tokita, S. Kawauchi, J. Watanabe, *Macromolecules*, 2000, **33**, 7420-7425; (b) K. Osada, M. Koike, H. Tagawa, M. Tokita, J. Watanabe, *Macromol. Chem. Phys.*, 2004, **205**, 1051-1057.
- 9 R. Ishige, T. Ishii, M. Tokita, M. Koga, S. Kang, J. Watanabe, *Macromolecules*, 2011, **44**, 4586-4588.
- 10 M. Al-Harhi, A. Sardashti, J. B. P. Soares, L. C. Simon, *Polymer*, 2007, **48**, 1954-1961.
- 11 K. A. Davis, K. Matyjaszewski, *Macromolecules*, 2000, **33**, 4039-4047.
- 12 Y. Tezuka, R. Komiya, *Macromolecules*, 2002, **35**, 8667-8669.
- 13 (a) S. Abraham, C.-S. Ha, I. Kim, *J. Polym. Sci., Part A: Polym. Chem.*, 2005, **43**, 6367-6378; (b) S. Hietala, S. Strandman, P. Jarvi, M. Torkkeli, K. Jankova, S. Hvilsted, H. Tenhu, *Macromolecules*, 2009, **42**, 1726-1732.
- 14 D. Wang, Z. Peng, X. Liu, Z. Tong, C. Wang, B. Ren, *Eur. Polym. J.*, 2007, **43**, 2799-2808.
- 15 (a) J. N. Israelachvili, D. J. Mitchell, B. W. Ninham, *J. Chem. Soc., Faraday Trans. 2*, 1976, **72**, 1525-1568; (b) J. Israelachvili, *Colloids Surf., A*, 1994, **91**, 1-8.
- 16 (a) A. Stein, S. G. Rudisill, N. D. Petkovich, *Chem. Mater.*, 2014, **26**, 259-276; (b) S. I. Stupp, L. C. Palmer, *Chem. Mater.*, 2014, **26**, 507-518.

- 17 K. T. Kim, J. Zhu, S. A. Meeuwissen, J. J. L. M. Cornelissen, D. J. Pochan, R. J. M. Nolte, J. C. M. van Hest, *J. Am. Chem. Soc.*, 2010, **132**, 12522-12524.
- 18 (a) L. Zhang, A. Eisenberg, *J. Am. Chem. Soc.*, 1996, **118**, 3168-3181; (b) Y. S. Yu, L. F. Zhang, A. Eisenberg, *Macromolecules*, 1998, **31**, 1144-1154.
- 19 (a) W. Helfrich, R. M. Servuss, *Il Nuovo Cimento D*, 1984, **3**, 137-151; (b) D. H. W. Hubert, M. Jung, P. M. Frederik, P. H. H. Bomans, J. Meuldijk, A. L. German, *Langmuir*, 2000, **16**, 8973-8979; (c) J. Pencer, G. F. White, F. R. Hallett, *Biophys. J.*, 2001, **81**, 2716-2728; (d) P. Saveyn, J. Cocquyt, P. Bomans, P. Frederik, M. De Cuyper, P. Van der Meeren, *Langmuir*, 2007, **23**, 4775-4781; (e) H. Yuan, C. Huang, S. Zhang, *Soft Matter*, 2010, **6**, 4571-4579; (f) S. A. Meeuwissen, K. T. Kim, Y. Chen, D. J. Pochan, J. C. M. van Hest, *Angew. Chem., Int. Ed.*, 2011, **50**, 7070-7073; (g) R. Salva, J.-F. Le Meins, O. Sandre, A. Brûlet, M. Schmutz, P. Guenoun, S. Lecommandoux, *ACS Nano*, 2013, **7**, 9298-9311.
- 20 Y. Murata, H. Iwasaki, M. Sasaki, K. Inaba, Y. Okamura, *Nature*, 2005, **435**, 1239-1243.
- 21 M. Sasaki, M. Takagi, Y. Okamura, *Science*, 2006, **312**, 589-592.



Scheme 1. Synthesis of (a) linear $AA_mBB_nAA_m$ from hydroxy-terminated BB_n and (b) cyclic $AA_{2m}BB_n$ from linear $tBA_mBB_n tBA_m$.

Table 1. Properties of the *t*Bu-protected and deprotected linear and cyclic block copolymers

<i>t</i> Bu-protected block copolymer						deprotected block copolymer ^a	
formula	ATRP time (min)	cyclization yield	M_n^b	M_p^c	PDI ^c	formula	M_n^b
linear <i>t</i> BA ₂₁ BB ₉ <i>t</i> BA ₂₁	15		2600–2800–2600	10800	1.16	linear AA ₂₁ BB ₉ AA ₂₁	1500–3000–1500
cyclic <i>t</i> BA ₃₁ BB ₁₀ ^d		70%	4000–3300	9200	1.24	cyclic AA ₃₃ BB ₁₀	2400–3400
linear <i>t</i> BA ₂₇ BB ₁₈ <i>t</i> BA ₂₇	30		3500–5700–3500	11000	1.33	linear AA ₂₅ BB ₁₄ AA ₂₅	1800–4700–1800
cyclic <i>t</i> BA ₅₄ BB ₁₆ ^d		38%	6900–5100	6100	1.28	cyclic AA ₅₁ BB ₁₈	3700–5900
linear <i>t</i> BA ₅₀ BB ₈ <i>t</i> BA ₅₀	60		6300–2700–6300	18700	1.16	linear AA ₄₄ BB ₉ AA ₄₄	3200–2900–3200
cyclic <i>t</i> BA ₉₁ BB ₈ ^d		74%	11700–2500	17500	1.17	cyclic AA ₁₀₀ BB ₉	7200–2900

^a M_p or PDI was not measured due to the insolubility of the AA segments in a solvent for SEC.

^b Molecular weights of the BB_{*n*}, *t*BA_{*m*}, and AA_{*m*} segments, and thus their numbers of the repeating units, were calculated by the peak areas of “a”, “j”, and “j”, respectively, with respect to “g” in the ¹H NMR spectra (Figure S3).

^c M_p and PDI were determined using calibration with polystyrene standards.

^d Cyclic *t*BA₃₁BB₁₀, *t*BA₅₄BB₁₆, and *t*BA₉₁BB₈ were synthesized from linear *t*BA₂₁BB₉*t*BA₂₁, *t*BA₂₇BB₁₈*t*BA₂₇, and *t*BA₅₀BB₈*t*BA₅₀, respectively.

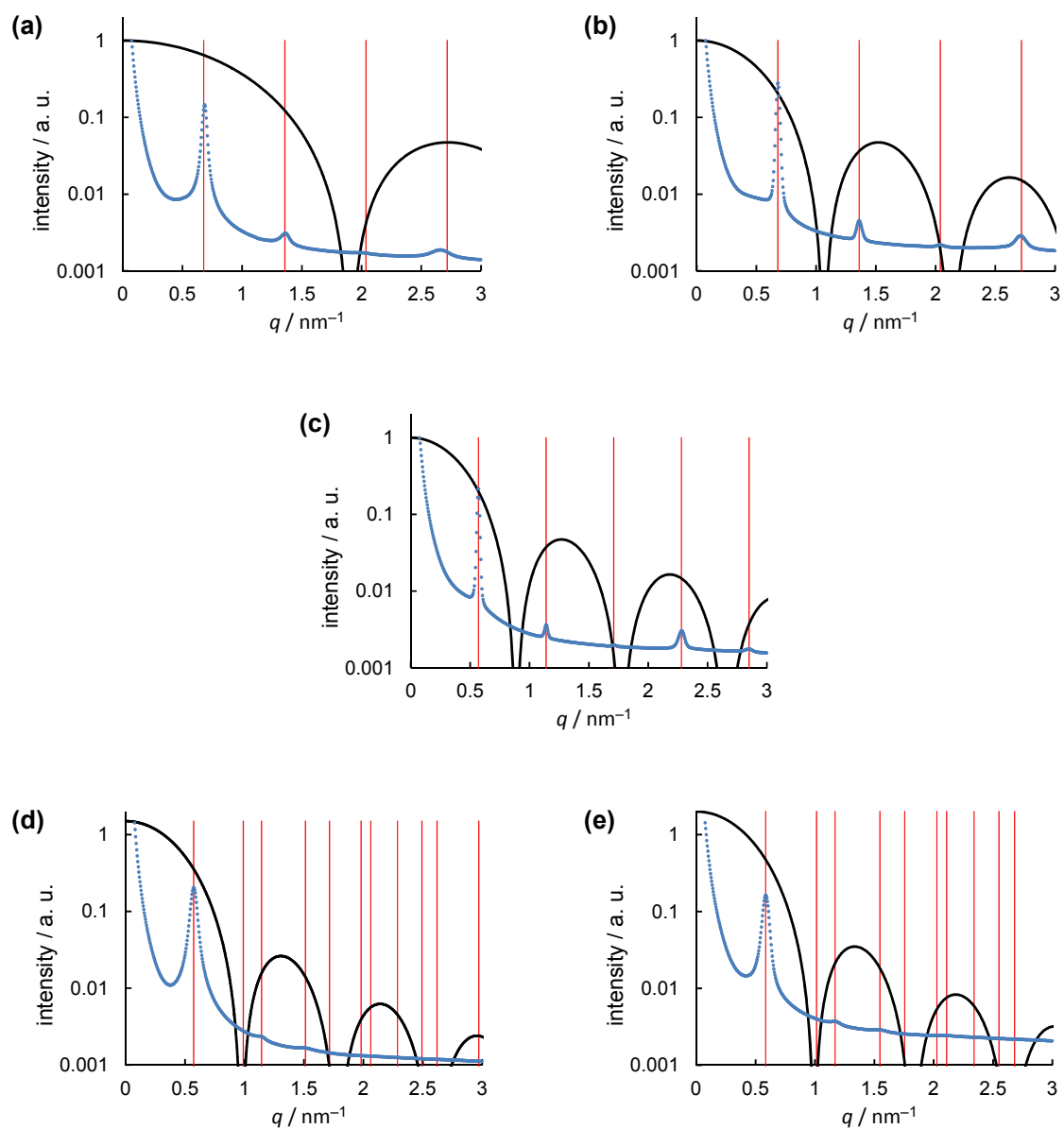


Figure 1. SAXS intensity profile (blue dots) measured for (a) linear $AA_{21}BB_9AA_{21}$, (b) cyclic $AA_{33}BB_{10}$, (c) cyclic $AA_{51}BB_{18}$, (d) linear $AA_{44}BB_9AA_{44}$, and (e) cyclic $AA_{100}BB_9$. Black curves and red lines are the square of the form factor and the lattice factor, respectively, calculated for (a–c) two-phase lamellar microdomains and (d) and (e) cylinder microdomains with the parameters shown in Table 2.

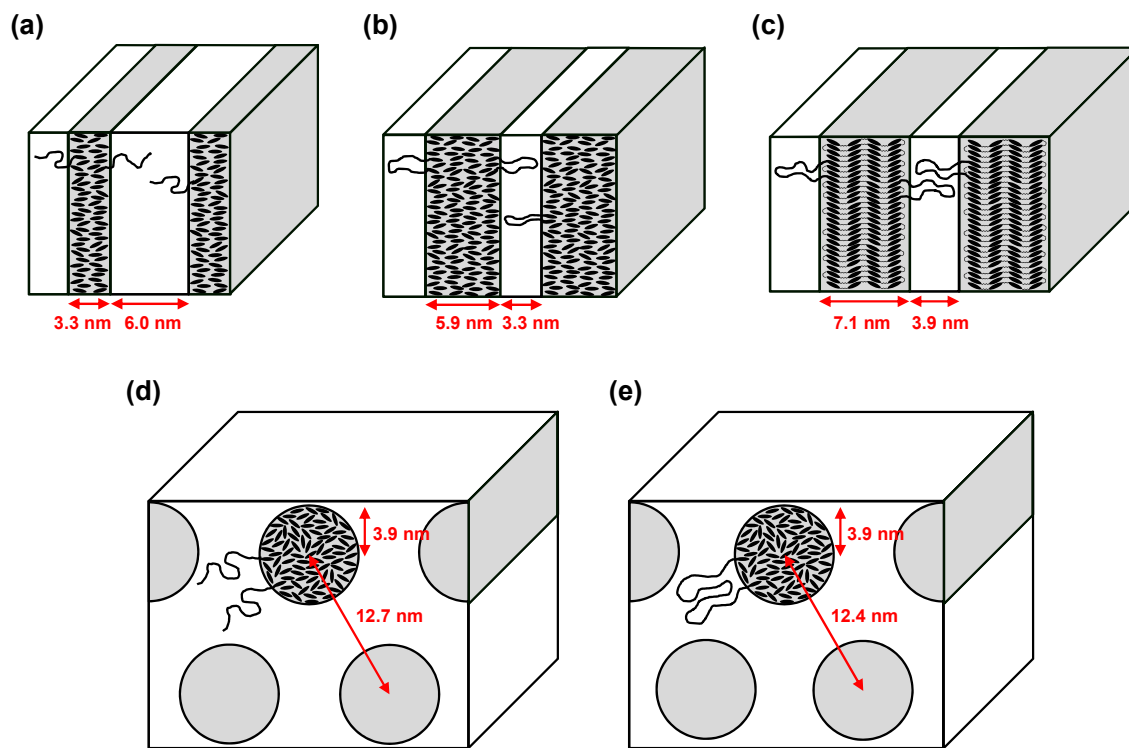


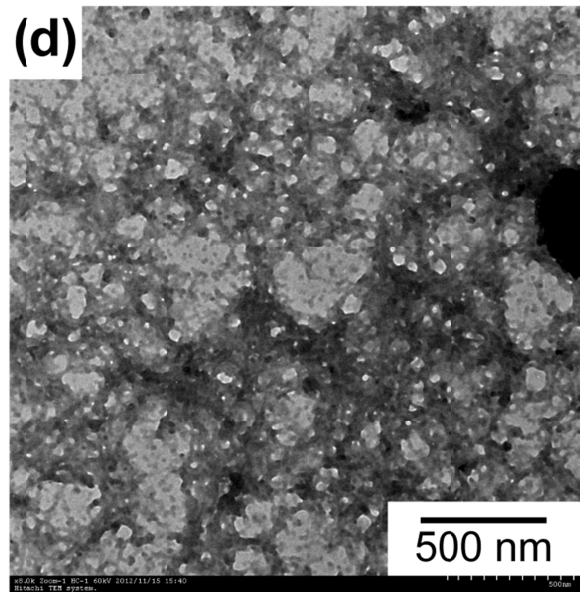
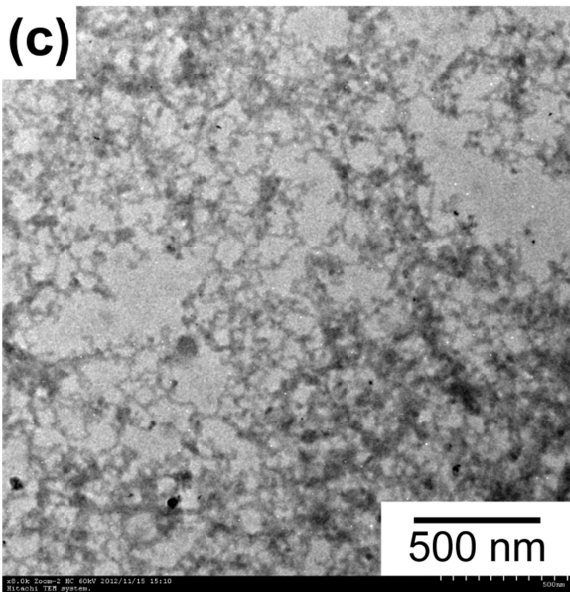
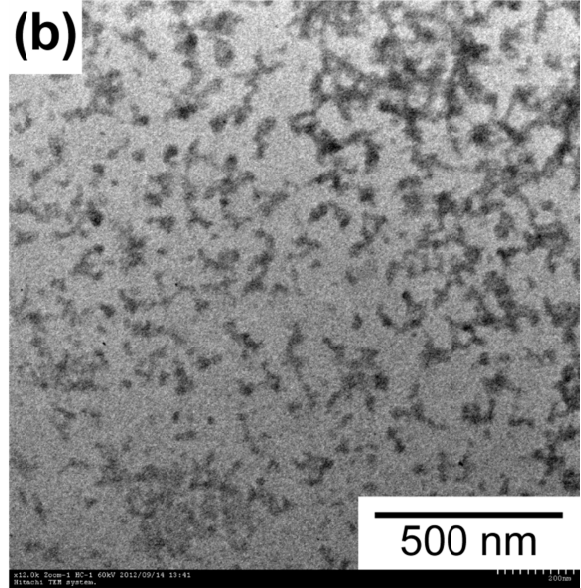
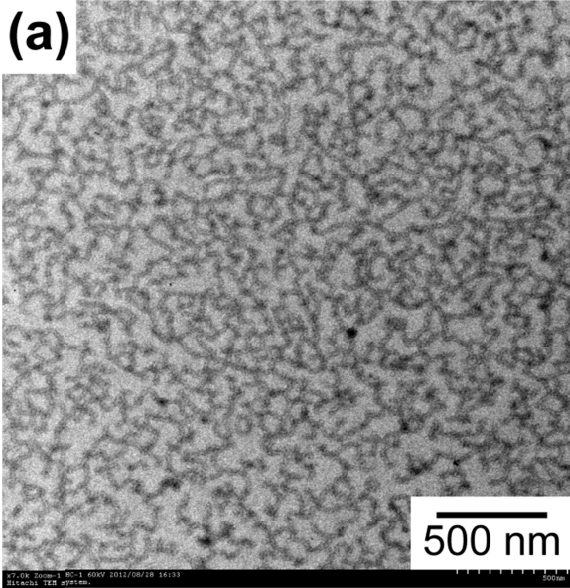
Figure 2. Phase separation models of (a) linear $AA_{21}BB_9AA_{21}$, (b) cyclic $AA_{33}BB_{10}$, (c) cyclic $AA_{51}BB_{18}$, (d) linear $AA_{44}BB_9AA_{44}$, and (e) cyclic $AA_{100}BB_9$.

Table 2. Solid morphology of linear AA₂₁BB₉AA₂₁, cyclic AA₃₃BB₁₀, cyclic AA₅₁BB₁₈, linear tBA₅₀BB₈tBA₅₀, linear AA₄₄BB₉AA₄₄, and cyclic AA₁₀₀BB₉ determined by SAXS

	structure	d ₁₀₀ (nm)	$\phi_{v, BBn}$	lamellar thickness or cylinder radius (nm)
linear AA ₂₁ BB ₉ AA ₂₁	lamellar	9.3	0.48 ^a	4.5 ^a
			0.35 ^b	3.3 ^b
cyclic AA ₃₃ BB ₁₀	lamellar	9.2	0.57 ^a	5.3 ^a
			0.64 ^b	5.9 ^b
cyclic AA ₅₁ BB ₁₈	lamellar with LC phases	11.0	0.60 ^a	6.6 ^a
			0.64 ^b	7.1 ^b
linear AA ₄₄ BB ₉ AA ₄₄	cylinder	11.0	0.30 ^a	3.6 ^a
			0.35 ^b	3.9 ^b
cyclic AA ₁₀₀ BB ₉	cylinder	10.7	0.27 ^a	3.4 ^a
			0.35 ^b	3.9 ^b

^a Based on the molecular weights and density of each segment

^b Based on the structure factors estimated from SAXS intensity



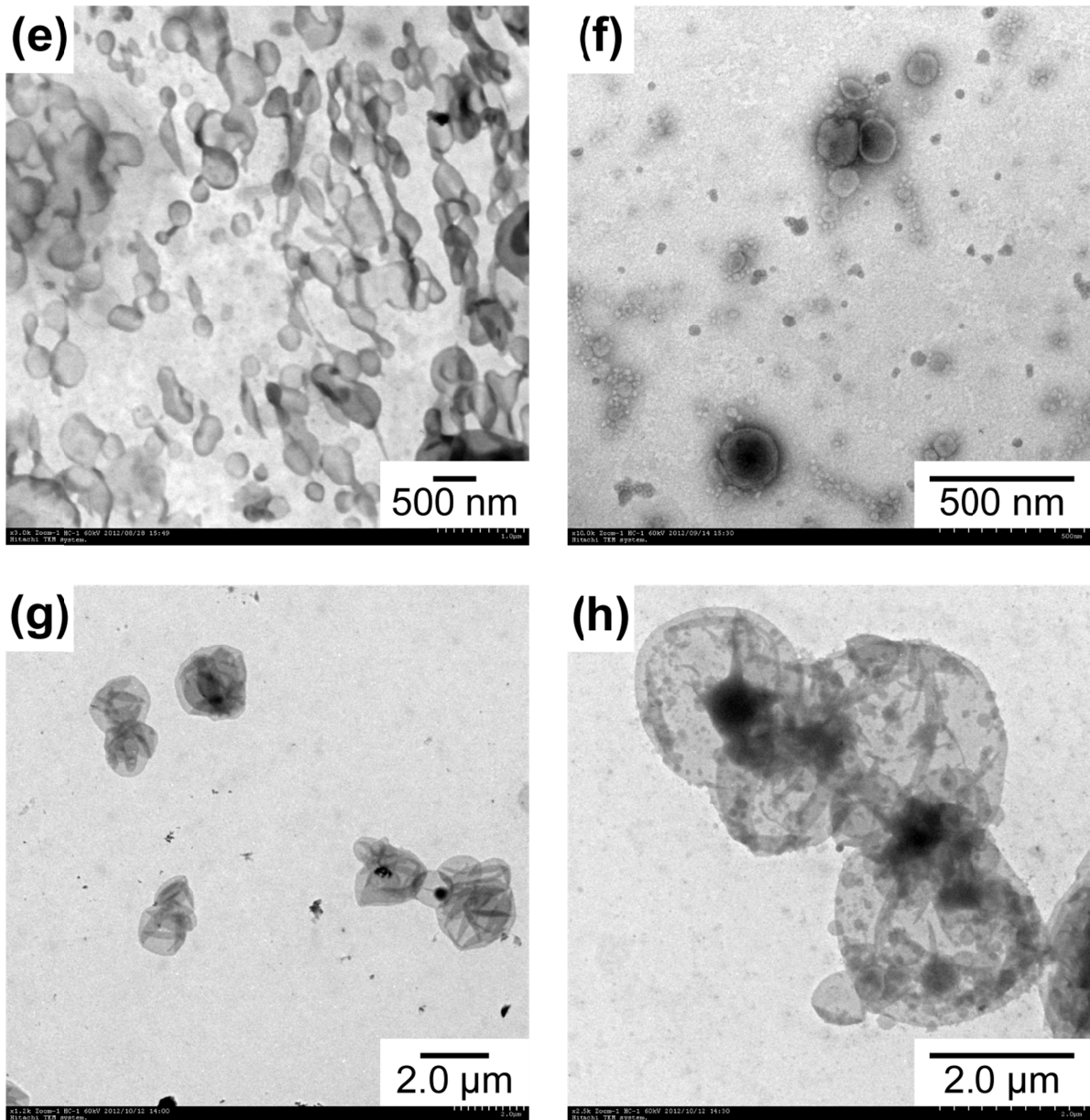
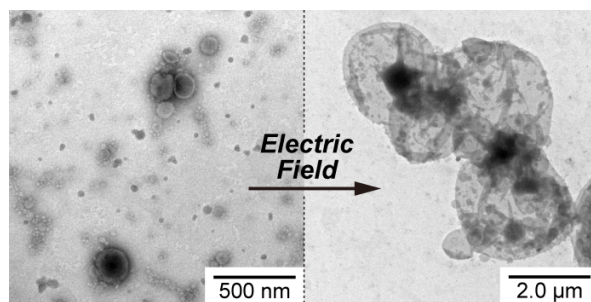


Figure 3. TEM images of self-assembled structures from linear $AA_{25}BB_{14}AA_{25}$ and cyclic $AA_{51}BB_{18}$ using an initial THF solution with a polymer concentration (c_0) of 1.0 and 10 mg/mL before and after applying an electric field (E) of 1.5 V/mm for 2 min. (a) Linear, $c_0 = 1.0$ mg/mL, before E . (b) Cyclic, $c_0 = 1.0$ mg/mL, before E . (c) Linear, $c_0 = 1.0$ mg/mL, after E . (d) Cyclic, $c_0 = 1.0$ mg/mL, after E . (e) Linear, $c_0 = 10$ mg/mL, before E , stained with TI-blue. (f) Cyclic, $c_0 = 10$ mg/mL, before E , stained with TI-blue. (g) Linear, $c_0 = 10$ mg/mL, after E . (h) Cyclic, $c_0 = 10$ mg/mL, after E .

TOC graphic



The effects of the macrocyclization of amphiphiles with a liquid crystalline segment were investigated in the solid state, and electric field-responsive cylindrical micelles and vesicles were self-assembled.